Shaping attosecond pulses by controlling the minima in high-order harmonic generation through alignment of CO_2 molecules

Cheng Jin,[1,2,*] Su-Ju Wang,[3] Xi Zhao,[3] Song-Feng Zhao,[4] and C. D. Lin[3]

[1]*Department of Applied Physics, Nanjing University of Science and Technology, Nanjing 210094, China*

[2]*State Key Laboratory of Transient Optics and Photonics, Xi'an Institute of Optics and Precision Mechanics, Chinese Academy of Sciences, Xi'an 710119, China*

[3]*J. R. Macdonald Laboratory, Department of Physics, Kansas State University, Manhattan, Kansas 66506, USA*

[4]*Key Laboratory of Atomic and Molecular Physics and Functional Materials of Gansu Province, College of Physics and Electronic Engineering, Northwest Normal University, Lanzhou 730070, China*

(Received 10 November 2019; published 23 January 2020)

We report a simple method for generating shaped attosecond pulses by using a CO_2 molecule. Unlike most other molecules, owing to its unique energy and angle dependence and the presence of deep minima in the photoionization transition dipole moment, the shape of harmonic spectra, especially the position and depth of minima, can be readily controlled by tuning the degree of alignment. The sensitive alignment dependence of the minima is due to the coherent interference of a laser-induced dipole from each molecule when CO_2 molecules are moderately aligned, but not when they are well aligned or when they are isotropically distributed. Such a sensitivity offers a simple way of controlling the spectral amplitude and phase of the generated harmonics and thus shaping the generated attosecond pulses, for example, producing structured attosecond pulses by splitting a single burst into two. We illustrate how such pulses are generated and how to characterize them. This method offers a simple way to shape attosecond pulses at the generation step. It can be easily implemented experimentally to generate attosecond pulses with strong phase variations for unique applications.

DOI: 10.1103/PhysRevA.101.013429

I. INTRODUCTION

In recent decades, high-order harmonic generation (HHG) resulting from the interaction of an intense infrared laser pulse with atoms and molecules has been widely studied [1–6]. Typically, harmonic signals exhibit a fast drop in intensity in the first few orders, followed by a long plateau region where the intensity of each order remains nearly the same until the cutoff, beyond which harmonics are continuous. Since harmonics are coherent, by synthesizing discrete plateau harmonics, an attosecond pulse train (APT) can be generated [7]. In the time domain, an APT appears as a train of bursts, each of which is of a duration of attoseconds with a well-behaved shape. Similarly, once the continuous harmonics are synthesized, in the time domain they would appear as an isolated attosecond pulse (IAP), with a well-behaved pulse envelope [8]. The IAPs and APTs generated in atomic gas targets have been widely used in numerous attosecond experiments [9,10] in the past decade.

Harmonics generated from an atom or molecule can be understood qualitatively with the three-step model: ionization, propagation, and recombination [11,12]. This model has been extended in the quantitative rescattering (QRS) theory [13–15], where the single-atom induced dipole can be expressed as a product of the complex returning electron wave packet $W(\omega)$ and the complex photorecombination (PR) transition dipole $d(\omega)$, where ω is the photon energy. Here $d(\omega)$ is the complex conjugate of the photoionization transition dipole, which is a property of the atom, and $W(\omega)$ is a property of the laser pulse. Thus, according to the QRS theory, a minimum in $|d(\omega)|^2$ would appear as a minimum in the harmonic spectrum. Changing the laser intensity or wavelength can only modify the smooth wave packet but not the position of the minimum in the harmonic spectra. This model has been well established for the harmonic spectra generated at the single-atom level. However, experimentally, the harmonic spectra are generated through the coherent buildup of harmonics from multiple atoms in the gas medium; then the position of the minimum observed in the harmonic spectra could be influenced by phase-matching conditions, especially at high laser intensities where the medium is modified by the laser. Ar, one of atomic targets, has been most extensively investigated (see e.g., Refs. [16–23]).

Harmonic spectra from molecules have also been extensively studied in the past two decades and the minima in the spectra have been of great interest. For each fixed-in-space molecule, the QRS theory also applies such that a minimum in the transition dipole moment would lead to a minimum in the harmonic spectra. Since molecules in the gas medium are randomly distributed or partially oriented, the generated harmonic spectra should be averaged over the angular distribution of molecules. In addition, in molecules, subshell binding energies are not well separated; thus harmonics can be generated from electrons in the highest occupied molecular orbital (HOMO) as well as from those in the inner-shell orbitals (HOMO-1, HOMO-2, and so on). The contribution to the harmonics from each subshell should be added coherently. At lower driving laser intensities, the harmonics

*Corresponding author: cjin@njust.edu.cn

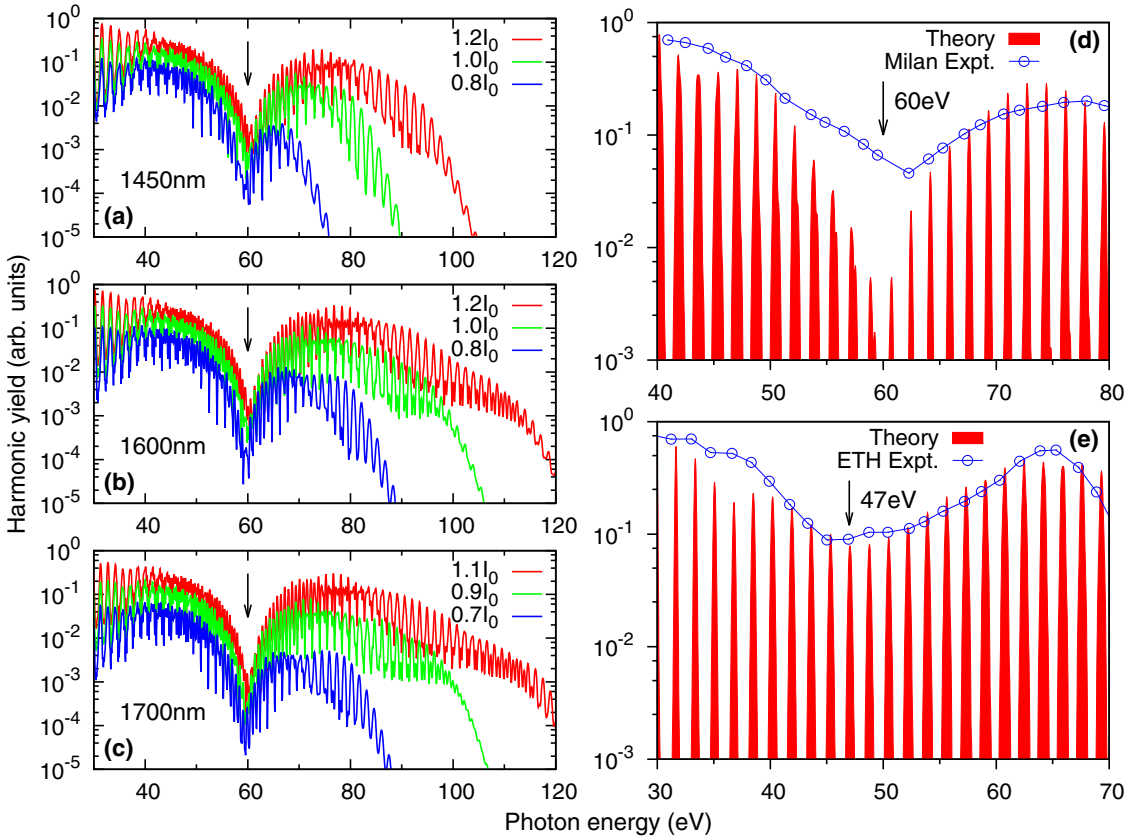

FIG. 1. (a)–(c) Simulated HHG spectra of aligned CO_2 molecules at different laser intensities and wavelengths (to be compared to Fig. 3 in Ref. [35]). In each figure, the laser intensity for the individual spectrum is gradually decreased from top to bottom. Laser intensities at the center of gas jet are indicated with $I_0 = 10^{14}$ W/cm^2. The degree of alignment by a pump laser is $\langle\cos^2\theta\rangle = 0.40$. (d) and (e) Comparison of theoretical HHG spectra and experimental ones of Vozzi *et al.* [35] and Rupenyan *et al.* [37] by using 1.45- and 1.46-μm lasers, respectively. In the simulations (d) $\langle\cos^2\theta\rangle = 0.40$ and (e) $\langle\cos^2\theta\rangle = 0.55$. The simulated results in (d) and (e) are smoothed by using the Gaussian function (with a full width at half maximum of 0.3 times the fundamental frequency) centered in the odd harmonics. Both the HOMO and two inner orbitals are included in the simulations. Arrows indicate the positions of the deep minima. See the text for additional laser parameters.

are generated from the HOMO only. According to the QRS theory, the position of the minimum is independent of either the laser intensity or the wavelength. At higher driving laser intensities, electrons from inner orbitals may also contribute to the harmonics and the position of the minimum would then depend upon the laser intensity. Both types of minima have been investigated extensively in the past decades, and the QRS theory has been able to reproduce these measurements in general [13–15]. In particular, CO_2 is one of the most popularly studied molecules (see, for example, Refs. [24–45]).

In spite of the extensive literature on HHG from CO_2 molecules, for years a well-known disparity has existed between the experiments of Vozzi *et al.* [35] and Rupenyan *et al.* [38]. They reported harmonic spectra for aligned CO_2 molecules with the degree of alignment $\langle\cos^2\theta\rangle$ near 0.6, where θ is the angle between the molecular axis and laser polarization. In Ref. [35] a sharp minimum was observed at 60 eV, yet in Ref. [38] a minimum was reported at 47 eV. In a theoretical simulation in Ref. [38], it was demonstrated that if the degree of alignment is 0.44, the minimum would occur at 60 eV, yet no experiment has ever been carried out on CO_2 molecules with such "poor" alignment with $\langle\cos^2\theta\rangle$ near 0.44.

In order to understand the origin of the discrepancy between the two experiments, we have carried out a "standard" QRS-type calculation. Through simulations, we have identified the plausible reason for the discrepancy in the position of the minimum of the two experiments. More importantly, we have further found that the position and the depth of the harmonic minimum are extremely sensitive to the alignment degree of CO_2, especially when molecules are only slightly aligned for $\langle\cos^2\theta\rangle$ as close to 0.40 if the molecules are aligned in parallel. Recall that there is no deep minimum in the interested spectral region in the harmonic spectra if the molecules are isotropically distributed, i.e., $\langle\cos^2\theta\rangle = 0.33$. We have traced the origin of such a strong alignment dependence to the strong angular dependence in the PR transition dipole moment of CO_2, in particular, the position of a minimum that is very deep and narrow and varies rapidly with the orientation of the molecular axis.

Recall that discrete harmonics can be synthesized to form an attosecond pulse train, while synthesizing continuous harmonics can form an isolated attosecond pulse. Once attosecond pulses are generated in the gas medium, it is rather difficult to reshape the pulse without a significant loss of its intensity. In view of the strong dependence of harmonic spectra on the alignment degree of CO_2, we propose to use this property as a practical method to generate shaped attosecond pulses. As reported below, in Sec. II we first show how we can

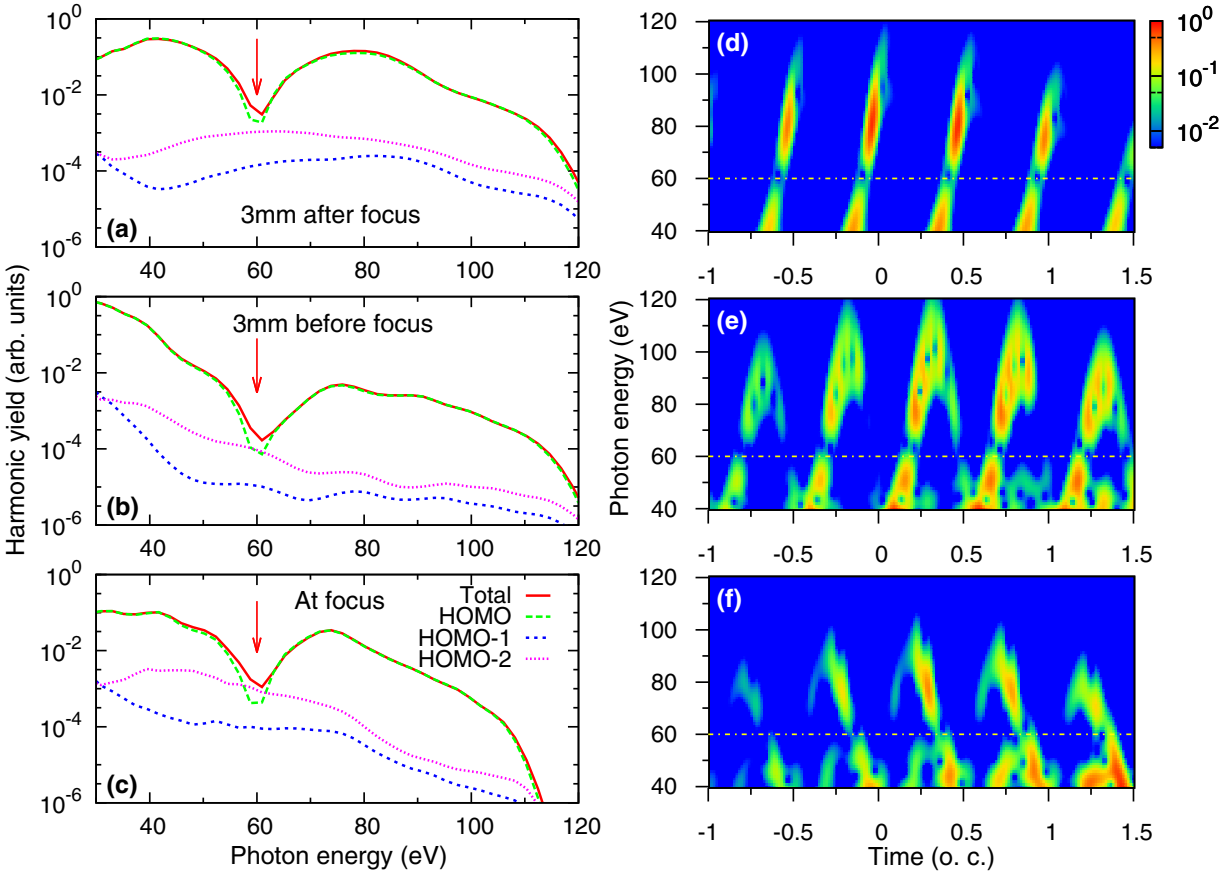

FIG. 2. (a)–(c) Simulated HHG spectra of aligned CO_2 molecules under different macroscopic conditions. In each figure, the total (HOMO, HOMO-1, and HOMO-2 together) spectra and individual HOMO, HOMO-1, and HOMO-2 spectra are plotted. To avoid the overlap of real HHG spectra, they are smoothed by using the method of Bézier curves. The laser wavelength is 1600 nm and the peak laser intensity at the center of the gas jet is fixed at 1.2×10^{14} W/cm^2. The positions of the gas jet with respect to the laser focus are changed as indicated. The other parameters are the same as those in Fig. 1(b). (d)–(f) Time-frequency analysis of macroscopic harmonic emissions at the off-axis position ($r = w_0/3$) of the exit plane under three different macroscopic conditions. Here w_0 is the beam waist of the generating laser. (o.c. means the optical cycle of the 1600-nm laser.)

interpret the discrepancy of the position of the minimum in two experiments and why such a difference is special to CO_2. We then show how the deep minimum in the harmonic spectra can be manipulated by fine-tuning the degree of alignment. In Sec. III we examine features of attosecond pulses in the time domain to demonstrate how they would vary with the degree of alignment. To confirm that such predictions indeed happen, we show how to determine the phases of such harmonics, focusing on the IAPs, with the phase retrieval method developed recently. The retrieval of spectral phases for shaped APTs is then addressed. We also discuss the possibility of generating shaped attosecond pulses experimentally. Section IV provides a short summary of the present work.

II. UNUSUAL FEATURES OF HARMONIC GENERATION FROM MODERATELY ALIGNED CO_2 MOLECULES

A. Origin of the difference in the harmonic spectra between two seemingly identical experiments

In earlier experiments, HHG of CO_2 molecules was typically carried out using laser wavelengths in the range of 800 nm to about 1.3 μm. To obtain a broad range of harmonics, higher laser intensities were often used. In such experiments, the position of the harmonic minimum tends to change with laser intensity resulting from the interference of harmonics from multiple orbitals [30,33]. In this work we focus on midinfrared driving lasers that have a wavelength longer than 1.4 μm. Because of the wavelength λ^2 scaling of the cutoff energy of harmonics, a broad spectral range can be obtained without very high laser intensity such that the primary contribution to HHG comes from the HOMO, with little from inner molecular orbitals. According to the QRS model, in this limit one expects the position of the harmonic minimum to be independent of either the laser intensity or wavelength. Indeed, in Ref. [35], harmonic spectra of CO_2 using wavelengths of 1450, 1600, and 1700 nm were reported with several intensities around 1.0×10^{14} W/cm^2. They found a clear deep minimum at about 60 eV and its position is independent of the laser intensity or wavelength. In a subsequent paper, Rupenyan *et al.* [38] reported the harmonic spectra from CO_2 molecules using wavelengths ranging from 1.16 to 1.46 μm, with an alignment factor of $\langle \cos^2 \theta \rangle = 0.54$–$0.64$. Their 1.46-$\mu$m laser parameters match with those used by Vozzi *et al.* [35], but the position of the

minimum was found to be around 47 eV. In both experiments, the molecules are aligned by a weaker pump laser and the harmonic spectra are generated by a more intense and shorter probe laser. The two lasers are polarized along the same direction and the molecular alignment degrees were both reported to be $\langle\cos^2\theta\rangle = 0.60$. Why do the positions of the minimum in the two experiments differ so much even with the same laser parameters and molecular alignment? In Ref. [38] a theoretical calculation similar to the QRS theory was carried out in the single-molecule response level, and the position of the minimum at $\langle\cos^2\theta\rangle = 0.60$ was found at 47 eV, in agreement with their experiment. Meanwhile, their simulation indicates that a minimum at 60 eV occurs if $\langle\cos^2\theta\rangle = 0.44$.

To investigate the discrepancy between the two experiments, we perform our standard QRS simulations. Different from the calculation of Rupenyan *et al.* [38], we use more accurate PR transition dipole matrix elements where the many-electron correlation has been better accounted for [46–48]. We also incorporate the propagation effect of harmonics generated in the gas medium. In the simulations, we choose a pulse with a duration of four optical cycles. The laser beam waist is assumed to be $w_0 = 35$ μm and the gas length is 0.5 mm. The gas, uniformly distributed in the interaction region, is placed at 3 mm after the laser focus. These parameters are close to those used experimentally by Vozzi *et al.* [35]. Our simulation results are displayed in Figs. 1(a)–1(c). They are to be compared to Fig. 3 of Ref. [35]. It is shown that the position of the minimum does not change with either the laser intensity or wavelength. In addition, as illustrated in Fig. 2, the position of the minimum does not change with the laser focusing condition; nor is it affected by the contribution from the HOMO-1 or HOMO-2 orbital, except that the depth of the minimum is reduced. Most importantly, however, our simulation suggests that a minimum occurs at 60 eV with the alignment degree of 0.40, close to 0.44, as used in Ref. [38].

To thoroughly compare our simulated spectra with those from Vozzi *et al.* [35], in Fig. 1(d) we display the envelope from each, including the propagation effect, by using an alignment factor of $\langle\cos^2\theta\rangle = 0.40$. The position of the minimum agrees quite well, but the depth of the minimum from the simulation is significantly deeper by one order. Such a discrepancy was not expected. Interestingly, when we compare our simulation with the data of Rupenyan *et al.* [38], not only the position of the minimum but also the envelope is in "perfect" agreement with data, when we use $\langle\cos^2\theta\rangle = 0.55$ [see Fig. 1(e)].

To figure out the possible factor(s) contributing to the discrepancy between our result and that from Vozzi *et al.* [35], we next look into the conditions of aligning lasers in the two experiments. Although the same $\langle\cos^2\theta\rangle = 0.6$ is utilized, three other parameters are different in the work of Vozzi *et al.* [35] and of Rupenyan *et al.* [38], including the peak intensity (4.0 vs 0.4×10^{13} W/cm^2), the temperature of gas jet (75 vs 40 K), and the pulse duration (100 vs 120 fs). In particular, to reach the cited high intensity, the aligning laser in Ref. [35] is focused. Aiming to test the effect of a focused aligning laser on harmonic generation, we carry out simulations that account for the laser intensity distribution at the gas jet position using three different beam waists to represent different degrees of focusing, where the peak intensity

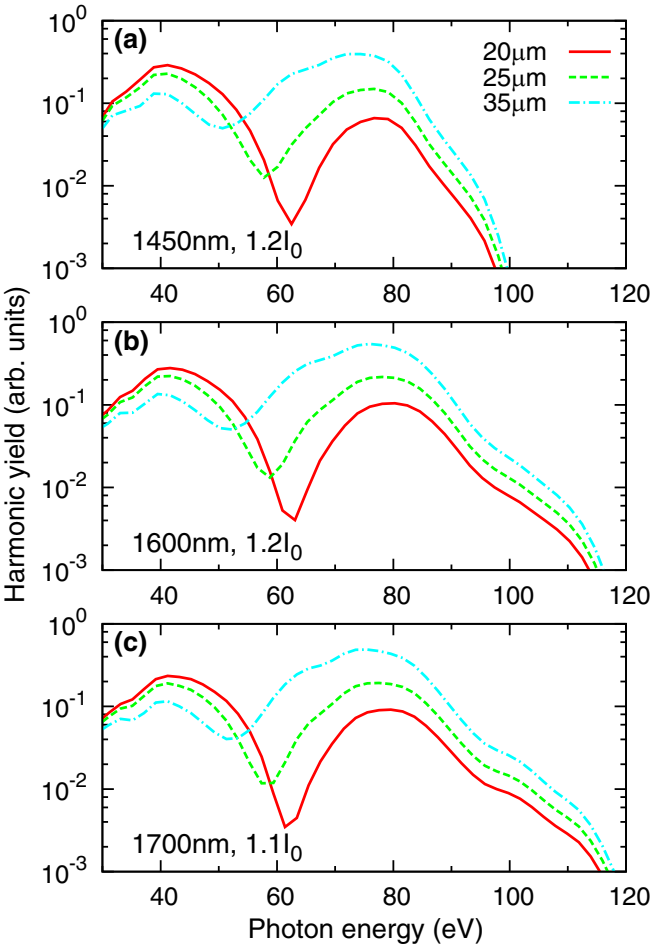

FIG. 3. Simulated HHG spectra of aligned CO_2 molecules under different focusing conditions of the pump laser. The spectra were smoothed by using Bézier curves. The wavelength of the pump laser is 800 nm, its intensity at the focus is fixed at 0.4×10^{14} W/cm^2, and its beam waist is varied as indicated in the figures. The 0.5-mm-long gas jet is located 3 mm after the laser focus. The wavelength and intensity (at the center of gas jet) of the probe laser are labeled in the figures. Other macroscopic conditions for the probe laser are the same as those in Fig. 1(b).

at the focus is 4×10^{13} W/cm^2. The simulation results are shown in Fig. 3. For the tight-focusing condition (beam waist $w_0 = 20$ μm) the harmonic minimum indeed occurs at about 60 eV. As the beam waist is increased, the position of the minimum is shifted to about 50 eV ($w_0 = 35$ μm), close to the 47 eV as observed by Rupenyan *et al.* [38]. Thus, the origin of the discrepancy in the position of the harmonic minimum between the two experiments is provided. Meanwhile, the discrepancy of a shallower minimum in the experimental data as compared to the much deeper minimum in the simulation in Fig. 1(d) can be understood. If the harmonic spectra were generated with molecules that are uniformly aligned with $\langle\cos^2\theta\rangle = 0.40$, then the harmonic minimum is expected to be as deep as the one seen in the simulation; however, no such measurements have been reported so far. In addition, the simulation also predicts that the position of the minimum shifts rapidly with a small change in the degree of alignment.

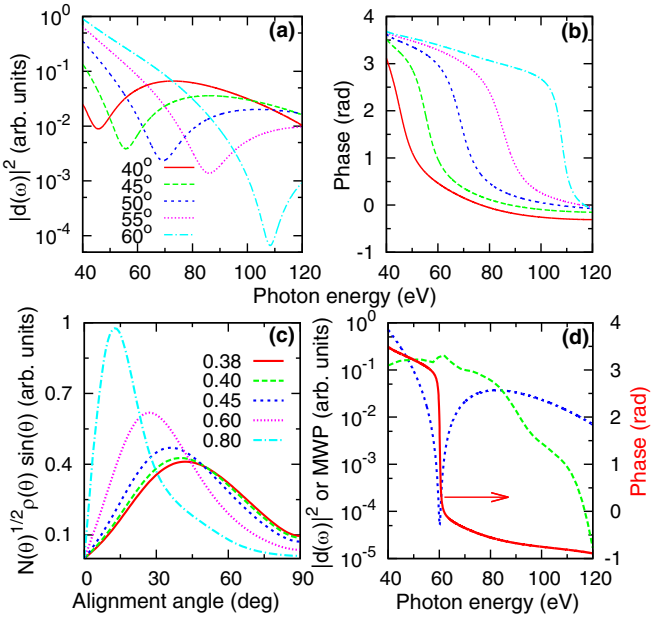

FIG. 4. (a) Photoionization transition dipole moment (the squared modulus) and (b) phase of fixed-in-space CO_2 molecules at selected alignment angles. Only the parallel component to the polarization direction of laser is shown. (c) Weighted angular distributions at different degrees of alignment by including the ionization rate $N(\theta)$ and alignment distribution $\rho(\theta)$. (d) Averaged photoionization transition dipole (the squared modulus, blue short-dashed line), phase of the dipole (red solid line), and the squared modulus of the macroscopic wave packet (MWP) (green long-dashed line) of the HOMO extracted from HHG spectra (1600 nm, $1.2I_0$) shown in Fig. 1(b).

This strong alignment dependence is due to the properties of the photoionization transition dipole moments in CO_2, as we further discuss below. This property offers the opportunity to control harmonic spectra using moderately aligned CO_2 molecules.

B. Efficient control of harmonic spectra by tuning the alignment of CO_2 molecules

The simulation of experimental harmonic spectra from partially aligned molecules involves the following steps. First, one calculates

$$d^{\parallel,\mathrm{avg}}(\omega,\alpha)=\int_0^{\pi} N(\theta)^{1/2} d^{\parallel}(\omega,\theta)\rho(\theta,\alpha)\sin\theta\, d\theta. \quad (1)$$

Here $d^{\parallel,\mathrm{avg}}(\omega,\alpha)$ is the averaged PR transition dipole, $N(\theta)$ is the ionization probability [49,50], $\rho(\theta,\alpha)$ is the alignment distribution (in the probe-laser frame) for the pump-probe angle α, and $d^{\parallel}(\omega,\theta)$ is the parallel (to the probe laser polarization) component of the PR transition dipole. A similar expression can be written for the perpendicular polarization direction. Here we consider $\alpha=0^{\circ}$ only, so there is no perpendicular polarization component. Note that the averaged transition dipole for each molecule is calculated coherently. With $d^{\parallel,\mathrm{avg}}(\omega,\alpha)$ calculated, in the second step the harmonics generated in the gas medium are obtained by solving the Maxwell's wave equations [51] to account for the effect of phase matching. Since $d(\omega)$ does not depend on the laser

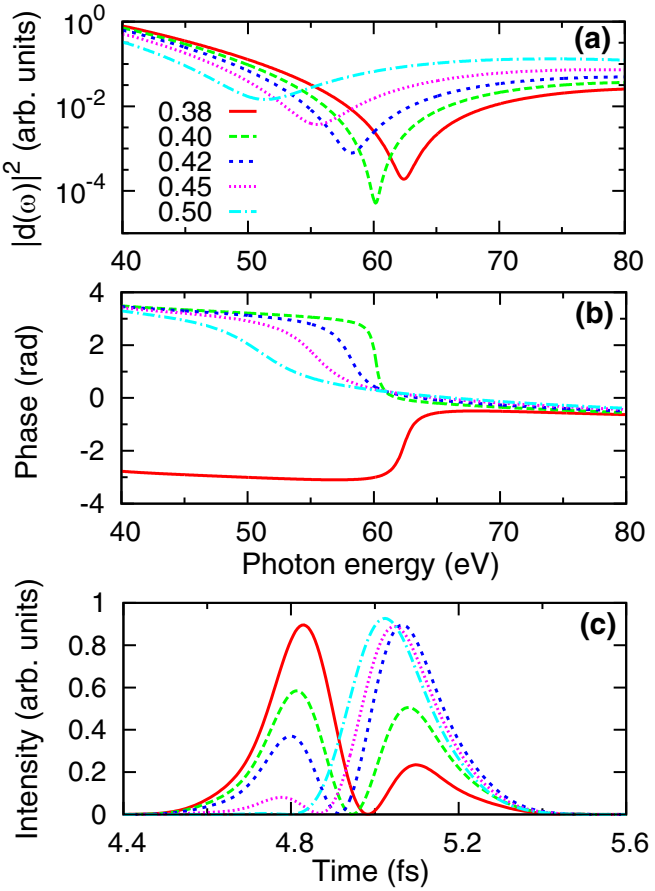

FIG. 5. (a) Averaged photoionization transition dipoles (the squared modulus) and (b) their phases, for the HOMO and parallel component only. Alignment degrees are indicated. (c) Attosecond pulses synthesized by off-axis ($r=w_0/3$) harmonics from 55 to 65 eV. A Gaussian envelope is applied to harmonics lower (or higher) than boundary ones. The results obtained from higher alignment degrees in (c) have been multiplied by several factors for easy comparison. The high harmonics are obtained by including both the HOMO and two inner orbitals; the other macroscopic conditions are the same as those in Fig. 1(b) for 1600 nm and $1.2I_0$.

[22], the observed harmonic spectrum can still be written in a product form, where the wave packet $W(\omega)$ in the QRS theory is replaced by a volume integrated wave packet $W'(\omega)$ which varies smoothly with photon energy. The macroscopic harmonic yields generated from a single molecular orbital can then be expressed as [51]

$$S_{\mathrm{h}}^{\parallel}(\omega,\alpha)\propto\omega^4|W'(\omega)|^2|d^{\parallel,\mathrm{avg}}(\omega,\alpha)|^2, \quad (2)$$

where $W'(\omega)$ is called a macroscopic wave packet. Thus, according to the QRS theory, the position of the minimum in the experimental harmonic spectra is determined by the angular distribution weighted transition dipole moment in Eq. (1).

Figure 4(a) shows the squared modulus of the PR transition dipole for a fixed-in-space CO_2 molecule at a few angles from 40° to 60°. Note that the position of the minimum and the amplitude change rapidly with the fixed-in-space angle. At the same time, the phase of the dipole undergoes a change

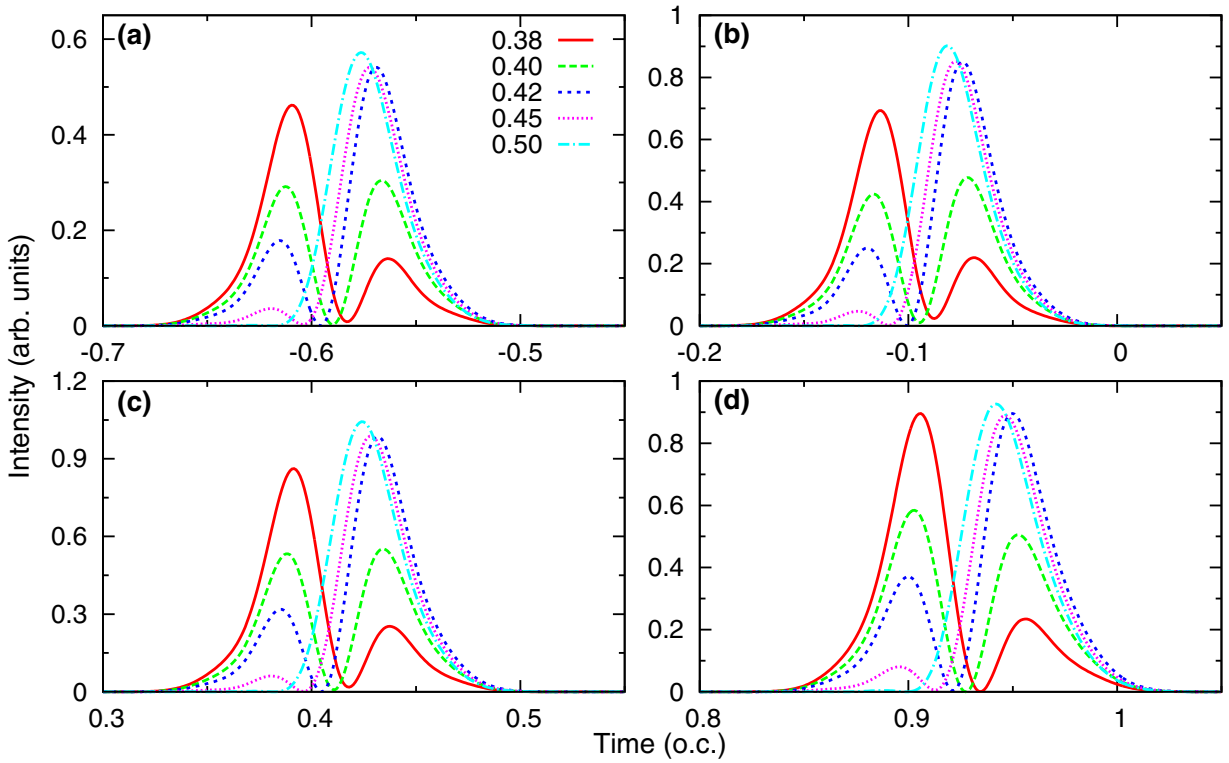

FIG. 6. Attosecond pulses shown in different half optical cycles by synthesizing off-axis ($r = w_0/3$) harmonics at the exit plane from 55 to 65 eV with only the molecular alignment distribution being adjusted. Gaussian envelope functions are applied to harmonics lower than 55 eV and higher than 65 eV. The results for $\langle\cos^2\theta\rangle = 0.45$ and 0.50 have been multiplied by 1/2 and 1/5 for easy comparison. (o.c. stands for the optical cycle of the 1600-nm laser.) Other macroscopic conditions are the same as those in Fig. 1(b).

of π within a small energy range; the narrower the minimum in Fig. 4(a), the smaller the energy range. Figure 4(d) shows what the averaged transition dipole and phase look like after the convolution with an angular distribution for the case of $\langle\cos^2\theta\rangle = 0.40$. In a narrow energy region near the minimum, both the amplitude and phase of the averaged transition dipole change dramatically in a narrow photon energy region. In contrast, the wave packet varies slowly with photon energy in the same energy region. Figure 4(c) shows the angular distributions weighted by the alignment-dependent ionization probability. While they do not change significantly for $\langle\cos^2\theta\rangle = 0.38$–$0.45$, Fig. 5(a) shows that the squared modulus of the averaged transition dipole changes significantly, where the position of the minimum moves from 63 to 55 eV, and in each case it is accompanied by a large change of phase, as shown in Fig. 5(b).

We emphasize that the averaged transition dipole shown in Fig. 4(d) is for molecules that are partially aligned along zero degree with respect to the probe laser. For $\langle\cos^2\theta\rangle = 0.4$, for example, the averaged transition dipole gets significant contributions from a broad angular range [see Fig. 4(c)]. In fact, for fixed-in-space molecules, the transition dipole can have a minimum only when the orientation angle of the molecule is within a range of 30°–60°. Thus the minima in Fig. 5(a) for different degrees of alignment are caused predominately by the coherent superposition of the transition dipole in that angular range. If the molecules are well aligned, then there would be no minimum in the averaged transition dipole. It can be seen already for $\langle\cos^2\theta\rangle = 0.50$, as shown in Fig. 5(a). This figure also shows why the position and depth of the minimum in the averaged transition dipole are so sensitive to the degree of alignment. We mention that Fig. 5(a) would mimic the harmonic spectra since the macroscopic wave packet is a smooth function of photon energy.

III. FEATURES OF ATTOSECOND PULSES SYNTHESIZED FROM A HARMONIC SPECTRUM THAT CONTAINS A DEEP MINIMUM

A. Efficient shaping of attosecond pulses

The preceding section focused on the harmonic spectra near the energy range where the minimum in the spectrum is very pronounced. Considering harmonics calculated from a 1600-nm laser with the duration of four optical cycles, we synthesize the ones covering from 55 to 65 eV which include the harmonic minimum. Figure 5(c) shows the time profile of the resulting attosecond pulses over one-half an optical cycle. (The time profiles at other half cycles are similar; see Fig. 6.) Here the time-domain attosecond pulses show two peaks within each half cycle, in contrast to attosecond pulses that have only one single peak if the harmonics do not contain a minimum. Very clearly, the relative contrast between the two peaks depends sensitively on the degree of alignment, consistent with the similar sensitive dependence of the harmonic spectra. This figure illustrates that one can change the temporal profile of attosecond pulses readily just by simply tuning the degree of alignment slightly. Note that the harmonic spectra were taken from Fig. 2(a) using the

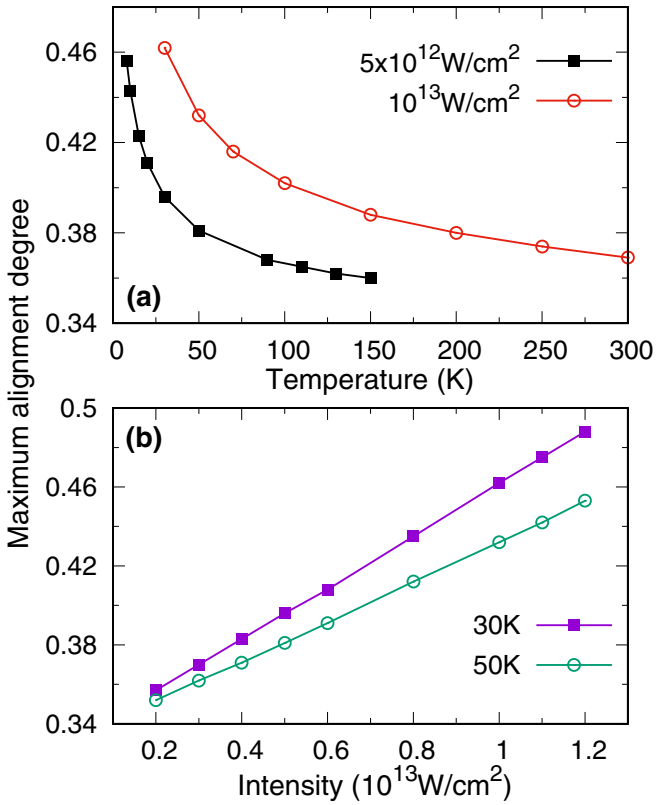

FIG. 7. Calculated maximum value of the alignment degree $\langle\cos^2\theta\rangle$ at the first half-revival as a function of (a) gas temperature and (b) laser intensity. The aligning laser has a wavelength of 800 nm and duration of 100 fs. The laser intensities in (a) and gas temperatures in (b) are fixed.

focusing condition that long-trajectory electrons have been removed through good phase matching.

The results presented in Fig. 5(c) are based on simulations with known alignment of molecules. One may argue that in experiments the precise alignment is not known such that the predicted shaping of attosecond pulses cannot be realized. This is not true. The degree of alignment can be readily adjusted by changing the input power of the pump laser. It is straightforward for experimentalists to locate the existence of the harmonic minimum without knowing the precise probe pulse intensity (since the position of the minimum does not depend on the intensity of the probing laser). To find the pump laser that would provide the deepest minimum one can just directly look at the harmonic spectrum as it is tuned. This is most easily carried out experimentally either by adding an iris in front of the pump laser to fine-tune its input power or by slightly adjusting the relative fraction of the pump and probe lasers' input power (or by somewhat adjusting the time delay between the two lasers). Figure 7 presents some simulation results. For a gas temperature of 30–50 K, a pump laser intensity below 1.2×10^{12} W/cm^2 can already cover the alignment in the desired range.

B. Characterization of shaped isolated attosecond pulses

To demonstrate shaped attosecond pulses in the time domain, it is best performed with isolated attosecond pulses. We illustrate this with theoretically constructed IAPs. As given in Eq. (2), an IAP can be theoretically constructed in the energy domain, for example, through multiplying a continuous Gaussian (or any) envelope by $d(\omega)$, which has the known amplitude and phase [as given in Figs. 5(a) and 5(b)].

The method of characterizing shaped attosecond pulses is not different from the one used to characterize IAPs generated in atoms. Both the amplitude and phase of the harmonics have to be known. The amplitude can be deduced from the photoelectron spectra for simple atoms ionized by the attosecond pulse alone, while the spectral phase can be determined by measuring the so-called streaking spectra generated by atoms in the combined field of the attosecond pulse and a moderately intense infrared laser. By analyzing the photoelectron spectra versus the time delay between the two pulses, the spectral phase of attosecond pulses has been reliably retrieved using the FROG-CRAB method. However, a better method, called PROBP [52], has been demonstrated since the latter removes the so-called central momentum approximation. (The PROBP-AC method [53] developed most recently is for broadband pulses, so it is not needed here.) In the following, we demonstrate how to retrieve the three shaped attosecond pulses that are generated from CO_2 molecules with slightly different degrees of alignment.

The electric field of an IAP (in the frequency domain) is described by $U(\omega)\exp[i\Phi(\omega)]$, where the amplitude is $U(\omega) = |d(\omega)|E_0 e^{-(\omega-\omega_0)^2/(\Delta\omega)^2}$ and the phase is directly taken from $d(\omega)$ as shown in Fig. 5(b). The central frequency ω_0 is set to be the dip position of the modulus of the transition dipole moment $d(\omega)$. The amplitudes of $U(\omega)$ are plotted in Figs. 8(a)–8(c) for the three cases of $\langle\cos^2\theta\rangle = 0.4$, 0.42, and 0.5 and the phases of $\Phi(\omega)$ and the corresponding temporal intensity envelopes of IAPs are shown in Fig. 9 (blue solid lines). We use such IAP fields combined with a moderate 800-nm laser to interact with the Ar atom, and the resulting photoelectron spectrograms are shown in Figs. 8(d)–8(f), simulated by using the strong-field approximation (SFA). A minimum band is formed near the central frequency subtracted by the ionization potential of argon, where electrons could hardly be emitted. The minimum positions for $\langle\cos^2\theta\rangle = 0.4$, 0.42, and 0.5 are around 44, 42, and 35 eV, respectively. Similar spectrograms have also been examined in Ref. [54], where the minimum band originates from the phase jump in the transition dipole moment of the target atom.

To retrieve the spectral phase of the IAP pulse from the spectrogram, we apply the PROBP method [52]. The spectral phase is expanded using B-spline basis functions. In addition to the size of the basis set (n) and the numbers of knots ($n+k$ in the case without multiplicity, where k is the order of B splines), which have been discussed in Ref. [52], the multiplicity and the distribution of knots are explored here. Including multiplicities in the end knots ensures that a nonzero value of the target function at the boundaries is taken into account. The multiplicity increases the size of the knot points from $n+k$ to $n+k+m_1+m_2$, where m_1 (m_2) is the multiplicity of the first (last) knot. In the following, we focus on $m_1 = m_2 = m$. Besides multiplicity, distribution of the knot points is important in order to effectively describe a drastic change in a target function without using too many basis

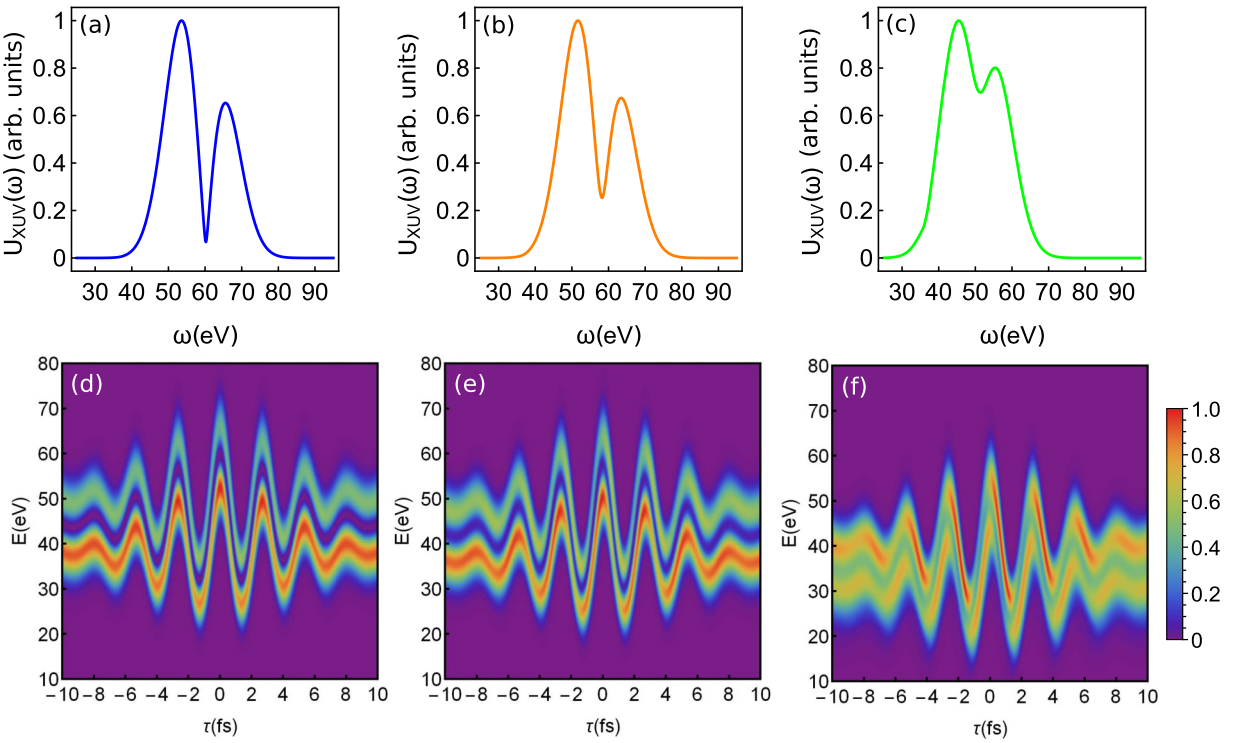

FIG. 8. Photoelectron spectrograms based on the SFA. Panels (a)–(c) show the actual IAP amplitudes used for generating the photoelectron spectrograms in (d), (e), and (f) for $\langle\cos^2\theta\rangle = 0.4$, 0.42, and 0.5, respectively. The IAP bandwidth $\Delta\omega = 10$ eV and $I_{\rm XUV} = 10^{12}$ W/cm^2. For the streaking field, we use $I_{\rm IR} = 10^{13}$ W/cm^2, $\lambda = 800$ nm, $\tau = 5.7$ fs, and $\phi_{\rm CEP} = \pi/2$. The spectrograms are rescaled to the range of [0, 1].

functions. A nonuniform placement of the knots is adopted in replacement of the uniform distribution used in Ref. [52]. The nonuniformity is controlled by a parameter α, which generates an exponentially increasing grid spacing as we move away from the central frequency of ω_0. With these two features included, the preoptimization process of the basis functions becomes a scan through the parameter set of $\{n, k, m, \alpha\}$. The most favorable basis set, which gives the optimum fitness within around 100 generations, is then used for the second-stage optimization to find the expansion coefficients of that basis set. For our retrieval, the number/order of B-spline basis functions are $n = 9$ and $k = 4$, and the multiplicity of the end knots is the same as the B-spline order, i.e., $m = 4$.

Figures 9(a), 9(c), and 9(e) show our retrieved results of the spectral phases for $\langle\cos^2\theta\rangle = 0.4$, 0.42, and 0.5 (orange dashed lines), respectively, in comparison with the input spectral phases (blue solid lines). The phase jumps in all three cases are reconstructed faithfully with the PROBP method except in the energy regions where the spectral amplitude is small. The input (blue solid lines) and the reconstructed temporal intensity profiles (orange dashed lines) calculated by using the input and retrieved spectral amplitudes and phases are shown in Figs. 9(b), 9(d), and 9(f). Good agreement is reached.

The phase characterization method demonstrated here for theoretical streaking spectra can be applied to analyze experimental data to retrieve shaped isolated attosecond pulses. Pulses similar to Figs. 9(b), 9(d), and 9(f) can be generated simply just by fine-tuning the alignment degree of the pump laser on CO_2 molecules. Changing the wavelength or the

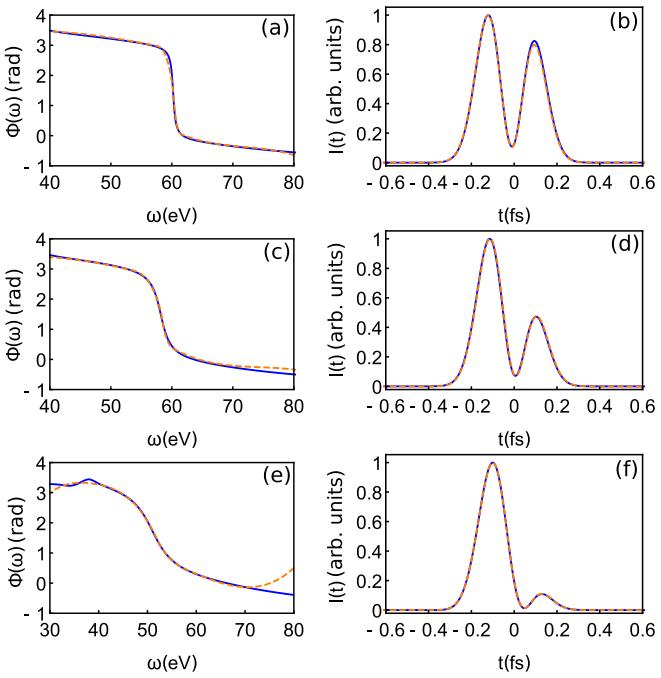

FIG. 9. The left column shows the input phases (blue solid lines) and the retrieved phase (orange dashed lines) for (a) $\langle\cos^2\theta\rangle = 0.4$, (c) $\langle\cos^2\theta\rangle = 0.42$, and (e) $\langle\cos^2\theta\rangle = 0.5$. The retrieved results reproduce the input spectral phases well except in the energy regions where the spectral amplitude is small. (b), (d), and (f) The corresponding intensity profiles using the input phase and the retrieved phase.

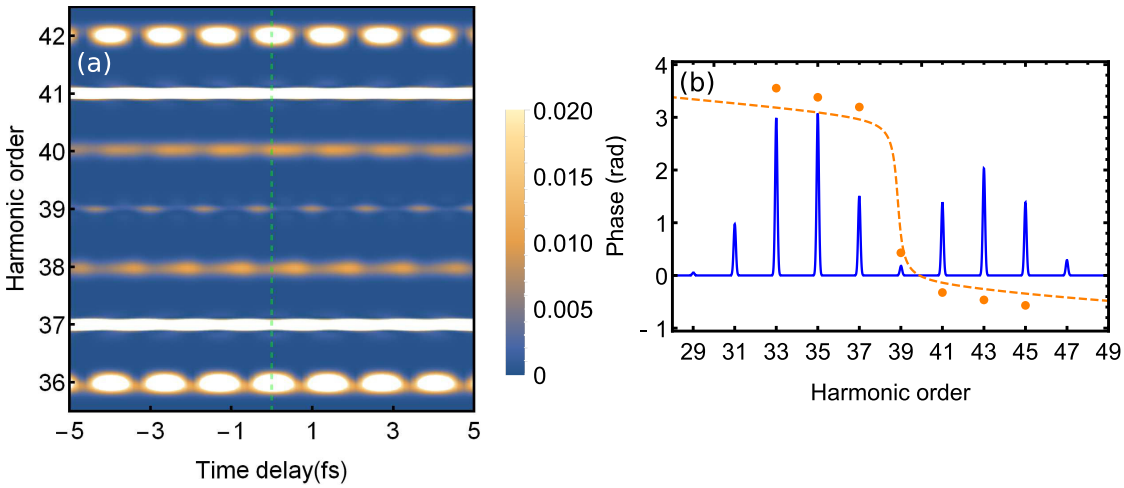

FIG. 10. (a) Photoelectron spectrum as a function of time delay. The green dashed line connects two sideband maxima, which can guide the eye to see the change of the location of the other sideband maxima. (b) Retrieved phase at odd harmonics shown as orange closed circles by using the RABITT method. Also shown is the input APT amplitudes (blue solid line) and phase (orange dashed line) for $\langle \cos^2\theta \rangle = 0.4$, which was used for generating the spectrum in (a). For the streaking field, we use $I_{\rm IR} = 10^{13}$ W/cm^2, $\lambda = 800$ nm, $\tau = 5.7$ fs, and $\phi_{\rm CEP} = \pi/2$. For easy comparison, we use the harmonic order (with respect to the 800-nm laser) to label photoelectron energy in (a), whose actual value equals the photon energy of the high harmonic minus the ionization potential of the target atom.

intensity of the probe laser would not change the shaped attosecond pulses. The strong variation of attosecond pulses generated here by slightly tuning the degree of molecular alignment can be viewed as a dramatic demonstration of coherent control since the effect relies on the coherence of harmonics generated from all molecules in the gas medium. The effect is dramatic because the phase of the transition dipole varies rapidly through π in CO_2 near the minimum of the transition dipole matrix element. Such a large phase change cannot be achieved using external phase modulators.

C. Retrieval of the phase of the shaped attosecond pulse train using the RABITT method

Here we show how to retrieve the phase of split attosecond pulse trains from experimental data to reconstruct their temporal profiles as displayed in Fig. 6. The so-called RABITT (reconstruction of attosecond beating by interference of two-photon transitions) [55] method is often used for retrieving the spectral phase of discrete harmonics. Experimentally, photoelectron spectra generated by the APT in the presence of a moderate IR pulse at different delay times are recorded. The electron spectra versus time delay would appear like those shown in Fig. 10(a). Besides the odd harmonics, even harmonics, called sidebands, would appear. The sideband signals show modulation which can be expressed as

$$S_{2q} = A_{2q} + B_{2q}\cos\left[2\omega_{\rm IR}t_d - (\varphi_{2q+1} - \varphi_{2q-1}) - \Delta_{2q}^{\rm atomic}\right]. \tag{3}$$

One can see that S_{2q} oscillates with frequency $2\,\omega_{\rm IR}$ as a function of the APT-IR time delay t_d. The atomic phase $\Delta_{2q}^{\rm atomic}$ is usually small compared to the phase of the harmonics and is neglected here. We thus can determine the phase difference $\varphi_{2q+1} - \varphi_{2q-1}$ between two adjacent odd harmonics by fitting the oscillation of the sideband signal.

In the absence of experimental streaking spectra for the shaped APT presented in this article, we generate the streaking spectra using the SFA. The infrared field is given by $E_{\rm IR}(t) = E_{\rm IR}e^{-t^2/\tau^2}\cos(\omega_{\rm IR}t + \phi_{\rm CEP})$, where $E_{\rm IR}$ is the field strength, $\omega_{\rm IR} = 2\pi/\lambda$ is the angular frequency, τ is the duration of the field, and $\phi_{\rm CEP}$ is the carrier envelope phase. For the shaped harmonic spectra, it is constructed by using the modulus of the averaged photoionization transition dipole in Fig. 5(a) multiplied by a discrete Gaussian envelope peaking at each odd harmonic of the 800-nm laser while keeping its phase [see the blue solid and orange dashed lines in Fig. 10(b)]. Applying the RABITT method, from Fig. 10(a), the retrieved phases at odd harmonics (orange closed circles) are shown in Fig. 10(b), which agree reasonably well with the input ones, and the fast π phase jump between harmonics 37 and 41 is demonstrated. Note that a better resolution of the retrieved phase jump can be obtained by using a longer-wavelength laser as the streaking field to reduce the IR photon energy between the orders [23].

IV. CONCLUSION

In summary, we have identified an alignment-induced enhancement of the minimum in high-order harmonic generation of CO_2 molecules. While minima in the harmonic spectra are ubiquitous in molecules, they are in general not very deep and the phase change of the harmonic across the minimum in general is less than π, for example, 2.7 rad at a Cooper minimum in Ar [23] and at 48 eV in CO_2 [29], and 2.6 rad in CH_3Cl [56]. It is also known that such a large phase change in general will generate moderately shaped attosecond pulses as in the case of Ar [23]. What is different in this study is that the harmonic minima are much deeper and the phase undergoes a change over π in a relatively small energy region. Unlike the minimum in Ar, the minima discussed here are significantly enhanced because of the interference of harmonic

minima from aligned molecules. Thus the position and depth of minima are very sensitive to the degree of alignment. This sensitivity offers a simple and practical method for shaping attosecond pulses by slightly changing the alignment degree of CO_2. This method works at a relatively small degree of alignment; thus it is easily realized in experiments.

While we have identified CO_2 as a working medium for efficient generation of shaped attosecond pulses, other molecules like N_2O [38], which have deep harmonic minima, probably work as an effective medium as well. In addition, we have considered parallel pump and probe polarizations in this article; a similar sensitive alignment dependence has been found for nonparallel configurations. In the latter cases, when the minimum occurs for the parallel polarization harmonics, the perpendicular components in general will not be at the minimum. Thus, by exploiting the nonparallel pump-probe geometry the present method may be used to generate polarized shaped attosecond pulses [57] that can be easily tuned with the alignment degree of molecules. Such shaped attosecond pulses would provide tools for probing ultrafast electron dynamics and provide different opportunities in attosecond sciences.

ACKNOWLEDGMENTS

We thank Dr. Caterina Vozzi and Dr. Giuseppe Sansone for fruitful discussions. C.J., X.Z., and S.-F.Z. were supported by National Natural Science Foundation of China under Grants No. 11774175, No. 91950102, No. 11834004, No. 11904192, and No. 11664035. S.-J.W., X.Z., and C.D.L. were supported by Chemical Sciences, Geosciences and Biosciences Division, Office of Basic Energy Sciences, Office of Science, U.S. Department of Energy under Grant No. DE-FG02-86ER13491.

[1] F. Krausz and M. Ivanov, Attosecond physics, Rev. Mod. Phys. **81**, 163 (2009).

[2] L.-Y. Peng, W.-C. Jiang, J.-W. Geng, W.-H. Xiong, and Q. Gong, Tracing and controlling electronic dynamics in atoms and molecules by attosecond pulses, Phys. Rep. **575**, 1 (2015).

[3] F. Calegari, G. Sansone, S. Stagira, C. Vozzi, and M. Nisoli, Advances in attosecond science, J. Phys. B **49**, 062001 (2016).

[4] J. P. Marangos, Development of high harmonic generation spectroscopy of organic molecules and biomolecules, J. Phys. B **49**, 132001 (2016).

[5] H. Yun, S. J. Yun, G. H. Lee, and C. H. Nam, High-harmonic spectroscopy of aligned molecules, J. Phys. B **50**, 022001 (2017).

[6] P. M. Kraus and H. J. Wörner, Perspectives of attosecond spectroscopy for the understanding of fundamental electron correlations, Angew. Chem. Int. Ed. **57**, 5228 (2018).

[7] P. M. Paul, E. S. Toma, P. Breger, G. Mullot, F. Augé, P. Balcou, H. G. Muller, and P. Agostini, Observation of a train of attosecond pulses from high harmonic generation, Science **292**, 1689 (2001).

[8] M. Hentschel, R. Kienberger, C. Spielmann, G. A. Reider, N. Milosevic, T. Brabec, P. Corkum, U. Heinzmann, M. Drescher, and F. Krausz, Attosecond metrology, Nature (London) **414**, 509 (2001).

[9] A. Kaldun, A. Blättermann, V. Stooß, S. Donsa, H. Wei, R. Pazourek, S. Nagele, C. Ott, C. D. Lin, J. Burgdörfer, and T. Pfeifer, Observing the ultrafast buildup of a Fano resonance in the time domain, Science **354**, 738 (2016).

[10] Y. Pertot, C. Schmidt, M. Matthews, A. Chauvet, M. Huppert, V. Svoboda, A. von Conta, A. Tehlar, D. Baykusheva, J.-P. Wolf, and H. J. Wörner, Time-resolved x-ray absorption spectroscopy with a water window high-harmonic source, Science **355**, 264 (2017).

[11] J. L. Krause, K. J. Schafer, and K. C. Kulander, High-Order Harmonic Generation from Atoms and Ions in the High Intensity Regime, Phys. Rev. Lett. **68**, 3535 (1992).

[12] P. B. Corkum, Plasma Perspective on Strong Field Multiphoton Ionization, Phys. Rev. Lett. **71**, 1994 (1993).

[13] A. T. Le, R. R. Lucchese, S. Tonzani, T. Morishita, and C. D. Lin, Quantitative rescattering theory for high-order harmonic generation from molecules, Phys. Rev. A **80**, 013401 (2009).

[14] C. D. Lin, A. T. Le, C. Jin, and H. Wei, Elements of the quantitative rescattering theory, J. Phys. B **51**, 104001 (2018).

[15] C. D. Lin, A. T. Le, C. Jin, and H. Wei, *Attosecond and Strong-Field Physics: Principles and Applications* (Cambridge University Press, Cambridge, 2018), pp. 209–213.

[16] H. J. Wörner, H. Niikura, J. B. Bertrand, P. B. Corkum, and D. M. Villeneuve, Observation of Electronic Structure Minima in High-Harmonic Generation, Phys. Rev. Lett. **102**, 103901 (2009).

[17] S. Minemoto, T. Umegaki, Y. Oguchi, T. Morishita, A. T. Le, S. Watanabe, and H. Sakai, Retrieving photorecombination cross sections of atoms from high-order harmonic spectra, Phys. Rev. A **78**, 061402(R) (2008).

[18] E. J. Takahashi, T. Kanai, Y. Nabekawa, and K. Midorikawa, 10 mJ class femtosecond optical parametric amplifier for generating soft x-ray harmonics, Appl. Phys. Lett. **93**, 041111 (2008).

[19] P. Colosimo, G. Doumy, C. I. Blaga, J. Wheeler, C. Hauri, F. Catoire, J. Tate, R. Chirla, A. M. March, G. G. Paulus, H. G. Muller, P. Agostini, and L. F. Dimauro, Scaling strong-field interactions towards the classical limit, Nat. Phys. **4**, 386 (2008).

[20] J. P. Farrell, L. S. Spector, B. K. McFarland, P. H. Bucksbaum, M. Gühr, M. B. Gaarde, and K. J. Schafer, Influence of phase matching on the Cooper minimum in Ar high-order harmonic spectra, Phys. Rev. A **83**, 023420 (2011).

[21] J. Higuet, H. Ruf, N. Thiré, R. Cireasa, E. Constant, E. Cormier, D. Descamps, E. Mével, S. Petit, B. Pons, Y. Mairesse, and B. Fabre, High-order harmonic spectroscopy of the Cooper minimum in argon: Experimental and theoretical study, Phys. Rev. A **83**, 053401 (2011).

[22] C. Jin, H. J. Wörner, V. Tosa, A. T. Le, J. B. Bertrand, R. R. Lucchese, P. B. Corkum, D. M. Villeneuve, and C. D. Lin, Separation of target structure and medium propagation effects in high-harmonic generation, J. Phys. B **44**, 095601 (2011).

[23] S. B. Schoun, R. Chirla, J. Wheeler, C. Roedig, P. Agostini, L. F. DiMauro, K. J. Schafer, and M. B. Gaarde, Attosecond Pulse Shaping around a Cooper Minimum, Phys. Rev. Lett. **112**, 153001 (2014).

[24] M. Lein, N. Hay, R. Velotta, J. P. Marangos, and P. L. Knight, Role of the Intramolecular Phase in High-Harmonic Generation, Phys. Rev. Lett. **88**, 183903 (2002).

[25] C. Vozzi, F. Calegari, E. Benedetti, J.-P. Caumes, G. Sansone, S. Stagira, M. Nisoli, R. Torres, E. Heesel, N. Kajumba, J. P. Marangos, C. Altucci, and R. Velotta, Controlling Two-Center Interference in Molecular High Harmonic Generation, Phys. Rev. Lett. **95**, 153902 (2005).

[26] T. Kanai, S. Minemoto, and H. Sakai, Quantum interference during high-order harmonic generation from aligned molecules, Nature (London) **435**, 470 (2005).

[27] N. Wagner, X. Zhou, R. Lock, W. Li, A. Wüest, M. Murnane, and H. Kapteyn, Extracting the phase of high-order harmonic emission from a molecule using transient alignment in mixed samples, Phys. Rev. A **76**, 061403(R) (2007).

[28] T. Kanai, E. J. Takahashi, Y. Nabekawa, and K. Midorikawa, Observing molecular structures by using high-order harmonic generation in mixed gases, Phys. Rev. A **77**, 041402(R) (2008).

[29] W. Boutu, S. Haessler, H. Merdji, P. Breger, G. Waters, M. Stankiewicz, L. J. Frasinski, R. Taieb, J. Caillat, A. Maquet, P. Monchicourt, B. Carre, and P. Salieres, Coherent control of attosecond emission from aligned molecules, Nat. Phys. **4**, 545 (2008).

[30] O. Smirnova, Y. Mairesse, S. Patchkovskii, N. Dudovich, D. Villeneuve, P. Corkum, and M. Yu. Ivanov, High harmonic interferometry of multi-electron dynamics in molecules, Nature (London) **460**, 972 (2009).

[31] P. Wei, P. Liu, J. Chen, Z. Zeng, X. Guo, X. Ge, R. Li, and Z. Xu, Laser-field-related recombination interference in high-order harmonic generation from CO_2 molecules, Phys. Rev. A **79**, 053814 (2009).

[32] H. J. Wörner, J. B. Bertrand, P. Hockett, P. B. Corkum, and D. M. Villeneuve, Controlling the Interference of Multiple Molecular Orbitals in High-Harmonic Generation, Phys. Rev. Lett. **104**, 233904 (2010).

[33] R. Torres, T. Siegel, L. Brugnera, I. Procino, J. G. Underwood, C. Altucci, R. Velotta, E. Springate, C. Froud, I. C. E. Turcu, S. Patchkovskii, M. Y. Ivanov, O. Smirnova, and J. P. Marangos, Revealing molecular structure and dynamics through high-order harmonic generation driven by mid-IR fields, Phys. Rev. A **81**, 051802(R) (2010).

[34] C. Jin, A. T. Le, and C. D. Lin, Analysis of effects of macroscopic propagation and multiple molecular orbitals on the minimum in high-order harmonic generation of aligned CO_2, Phys. Rev. A **83**, 053409 (2011).

[35] C. Vozzi, M. Negro, F. Calegari, G. Sansone, M. Nisoli, S. De Silvestri, and S. Stagira, Generalized molecular orbital tomography, Nat. Phys. **7**, 822 (2011).

[36] K. Kato, S. Minemoto, and H. Sakai, Suppression of high-order-harmonic intensities observed in aligned CO_2 molecules with 1300-nm and 800-nm pulses, Phys. Rev. A **84**, 021403(R) (2011).

[37] A. Rupenyan, P. M. Kraus, J. Schneider, and H. J. Wörner, Quantum interference and multielectron effects in high-harmonic spectra of polar molecules, Phys. Rev. A **87**, 031401(R) (2013).

[38] A. Rupenyan, P. M. Kraus, J. Schneider, and H. J. Wörner, High-harmonic spectroscopy of isoelectronic molecules: Wavelength scaling of electronic-structure and multielectron effects, Phys. Rev. A **87**, 033409 (2013).

[39] M. Qin, X. Zhu, Y. Li, Q. Zhang, P. Lan, and P. Lu, Probing rotational wave-packet dynamics with the structural minimum in high-order harmonic spectra, Opt. Express **22**, 6362 (2014).

[40] H. Yun, K.-M. Lee, J. H. Sung, K. T. Kim, H. T. Kim, and C. H. Nam, Resolving Multiple Molecular Orbitals Using Two-Dimensional High-Harmonic Spectroscopy, Phys. Rev. Lett. **114**, 153901 (2015).

[41] B. D. Bruner, Z. Mašín, M. Negro, F. Morales, D. Brambila, M. Devetta, D. Faccialà, A. G. Harvey, M. Ivanov, Y. Mairesse, S. Patchkovskii, V. Serbinenko, H. Soifer, S. Stagira, C. Vozzi, N. Dudovich, and O. Smirnova, Multidimensional high harmonic spectroscopy of polyatomic molecules: Detecting sub-cycle laser-driven hole dynamics upon ionization in strong mid-IR laser fields, Faraday Discuss. **194**, 369 (2016).

[42] N. Suárez, A. Chacón, J. A. Pérez-Hernández, J. Biegert, M. Lewenstein, and M. F. Ciappina, High-order-harmonic generation in atomic and molecular systems, Phys. Rev. A **95**, 033415 (2017).

[43] M. Ruberti, P. Decleva, and V. Averbukh, Multi-channel dynamics in high harmonic generation of aligned CO_2: *ab initio* analysis with time-dependent B-spline algebraic diagrammatic construction, Phys. Chem. Chem. Phys. **20**, 8311 (2018).

[44] T. Gorman, T. Scarborough, P. Abanador, F. Mauger, D. Kiesewetter, P. Sándor, S. Khatri, K. Lopata, K. J. Schafer, P. Agostini, M. Gaarde, and L. DiMauro, Probing the interplay between geometric and electronic-structure features via high-harmonic spectroscopy, J. Chem. Phys. **150**, 184308 (2019).

[45] F. Mauger, P. M. Abanador, T. D. Scarborough, T. T. Gorman, P. Agostini, L. F. DiMauro, K. Lopata, K. J. Schafer, and M. B. Gaarde, High-harmonic spectroscopy of transient two-center interference calculated with time-dependent density-functional theory, Struct. Dyn. **6**, 044101 (2019).

[46] R. R. Lucchese and V. McKoy, Studies of differential and total photoionization cross sections of carbon dioxide, Phys. Rev. A **26**, 1406 (1982).

[47] C. Jin, A. T. Le, S. F. Zhao, R. R. Lucchese, and C. D. Lin, Theoretical study of photoelectron angular distributions in single-photon ionization of aligned N_2 and CO_2, Phys. Rev. A **81**, 033421 (2010).

[48] A. T. Le, R. R. Lucchese, M. T. Lee, and C. D. Lin, Probing Molecular Frame Photoionization via Laser Generated High-Order Harmonics from Aligned Molecules, Phys. Rev. Lett. **102**, 203001 (2009).

[49] X. M. Tong, Z. X. Zhao, and C. D. Lin, Theory of molecular tunneling ionization, Phys. Rev. A **66**, 033402 (2002).

[50] S. F. Zhao, C. Jin, A. T. Le, T. F. Jiang, and C. D. Lin, Determination of structure parameters in strong-field tunneling ionization theory of molecules, Phys. Rev. A **81**, 033423 (2010).

[51] C. Jin, A. T. Le, and C. D. Lin, Medium propagation effects in high-order harmonic generation of Ar and N_2, Phys. Rev. A **83**, 023411 (2011).

[52] X. Zhao, H. Wei, Y. Wu, and C. D. Lin, Phase-retrieval algorithm for the characterization of broadband single attosecond pulses, Phys. Rev. A **95**, 043407 (2017).

[53] W.-W. Yu, X. Zhao, H. Wei, S.-J. Wang, and C. D. Lin, Method for spectral phase retrieval of single attosecond pulses utilizing the autocorrelation of photoelectron streaking spectra, Phys. Rev. A **99**, 033403 (2019).

[54] V. S. Yakovlev, J. Gagnon, N. Karpowicz, and F. Krausz, Attosecond Streaking Enables the Measurement of Quantum Phase, Phys. Rev. Lett. **105**, 073001 (2010).

[55] H. G. Muller, Reconstruction of attosecond harmonic beating by interference of two-photon transitions, Appl. Phys. B **74**, s17 (2002).

[56] T. D. Scarborough, T. T. Gorman, F. Mauger, P. Sándor, S. Khatri, M. B. Gaarde, K. J. Schafer, P. Agostini, and L. F. DiMauro, Full characterization of a molecular cooper minimum using high-harmonic spectroscopy, Appl. Sci. **8**, 1129 (2018).

[57] P.-C. Huang, C. Hernández-García, J.-T. Huang, P.-Y. Huang, C.-H. Lu, L. Rego, D. D. Hickstein, J. L. Ellis, A. Jaron-Becker, A. Becker, S.-D. Yang, C. G. Durfee, L. Plaja, H. C. Kapteyn, M. M. Murnane, A. H. Kung, and M.-C. Chen, Polarization control of isolated high-harmonic pulses, Nat. Photon. **12**, 349 (2018).